

RSC Advances



This is an *Accepted Manuscript*, which has been through the Royal Society of Chemistry peer review process and has been accepted for publication.

Accepted Manuscripts are published online shortly after acceptance, before technical editing, formatting and proof reading. Using this free service, authors can make their results available to the community, in citable form, before we publish the edited article. This *Accepted Manuscript* will be replaced by the edited, formatted and paginated article as soon as this is available.

You can find more information about *Accepted Manuscripts* in the [Information for Authors](#).

Please note that technical editing may introduce minor changes to the text and/or graphics, which may alter content. The journal's standard [Terms & Conditions](#) and the [Ethical guidelines](#) still apply. In no event shall the Royal Society of Chemistry be held responsible for any errors or omissions in this *Accepted Manuscript* or any consequences arising from the use of any information it contains.

High Performance Supercapacitors Based On Ternary Graphene/Au/Polyaniline (PANI) Hierarchical Nanocomposites

Luyan Wang^{1*}, Ting Wu¹, Sen Du¹, Meishan Pei¹, Wenjuan Guo¹ and Suying Wei^{2*}

¹School of Chemistry and Chemical Engineering, University of Jinan, Jinan 250022, China

²Department of Chemistry and Biochemistry, Lamar University, Beaumont, TX, USA

Corresponding Author's contact information:

E-mail: chm_wangly@ujn.edu.cn

Tel: +86-531-89736800; Fax: +86-531-87161600

Abstract

A ternary graphene/Au/PANI nanocomposite (GAP) is designed and fabricated via a facile two-step approach: Au nanoparticles dispersed on graphene sheets are achieved by a hydrothermal method, followed by coating with PANI through in situ polymerization process. Electrochemical measurements demonstrate that the specific capacitance of the resulting ternary composite is $572 \text{ F}\cdot\text{g}^{-1}$ at a current density of $0.1 \text{ A}\cdot\text{g}^{-1}$ using a three-electrode system, which is significantly higher than that of pure PANI and binary graphene-PANI composite. In addition, over 88.54 % of the initial capacitance can be retained after repeating tests for 10000 cycles, demonstrating a high cycling stability. The extraordinary electrochemical performance of the ternary GAP nanocomposite is attributed to its well-designed nanostructure and the synergistic effects among individual components.

1. INTRODUCTION

The fast-growing markets for portable electronic devices, such as notebook computers, mobile phones and personal memory cards, and their development trend of being small, light-weight, and flexible have brought about an ever-rising and urgent demand for environmentally friendly electrochemical energy storage and conversion systems, including batteries, fuel cells, capacitors, and supercapacitors.^[1-3] Among them, supercapacitors, also known as electrochemical capacitors or ultracapacitors, have been intensively studied because of their high power density, long cycle life (>10000 cycles), and rapid charging-discharging rates.^[1,2,4]

It is well known that flexible conducting polymers are generally considered to be ideal electrode materials for flexible energy storage devices.^[5-8] Among different conducting polymers, polyaniline (PANI) has attracted persistent attention owing to its high pseudocapacitance, light weight, low cost, controllable electrical conductivity, high energy density, environmental friendliness, facile synthesis^[9-11] and fast doping/dedoping rate during charge/discharge process.^[5,6,12,13] However, the main shortcoming of PANI as a supercapacitor electrode is the poor cycling stability derived from the volumetric changes during the doping/de-doping process.^[4,14-18] In order to overcome this problem, it is necessary to combine another material to enhance cycling stability. Graphene is a single-atom-thick, two-dimensional sheet of sp^2 -hybridized carbon atoms arranged in a honeycomb crystal structure with exceptionally high strength, surface area, thermal conductivity, and electronic conductivity.^[19-21] Composites of PANI with graphene are promising because

graphene is an excellent substrate to host the active polymer.^[22] In addition, dramatic improvements in their properties and performances can be achieved due to the synergistic effect between the two components. In essence, due to the high doping-dedoping rate during charge-discharge cycles, PANI can generally promote the electrochemical capacitance of any carbonaceous material. Aside from its inherent benefits such as ease of synthesis, low-cost and large pseudocapacitance, PANI can serve as an intercalated spacer to further enhance the host surface area. Graphene can serve as a stable and underlying conductive network, where good electrical conductivity and improved cycling stability can be achieved. Such hybrid PANI-graphene nanostructures can be beneficial in the development of next-generation electrochemical energy storage devices with a long cycle life.

However, in order to achieve full electrode utilization, sufficient battery power, and fast discharge/charge rates, the electrical conductivity of graphene/PANI needs to be further improved. It is well-known that the electrical conductivity of electrodes can be improved through the formation of a conductive percolation network by the incorporation of metal nanoparticles (NPs). Incorporation of metal NPs into electrodes may increase the specific capacity of metal-embedded electrodes by about 10~30% as compared to electrodes without them.^[23,24] Among the metal NPs, Au nanoparticle, with high conductivity, stability, flexibility, affinity to most metal oxides and low melting temperature (for Au NPs), is an excellent candidate.^[25,26] In this context, hierarchically ternary composites consisted of carbon nanomaterials, conducting polymers and transition metal nanoparticles have been explored and

demonstrated improvement in the electrochemical performance, which provides a new direction for the fabrication of the next generation high performance electrochemical electrodes. Based on the above, it is of great interests to study the ternary graphene/AuNPs/PANI nanocomposites for supercapacitors. To the best of our knowledge, very few studies on the synthesis of this intriguing ternary nanostructure have been reported so far.

In the present paper, we reported a facile two-step method for the synthesis of a ternary graphene/AuNPs/PANI (GAP) nanocomposite as an advanced capacitor material. Both graphene oxide deoxygenation and Au nanoparticles loading were achieved during the hydrothermal process, leading to the formation of binary graphene/Au (GA) hybrid. Subsequently, an in situ polymerization strategy was adopted for further coating polyaniline on the surface of GA sheets. This unique ternary GAP demonstrated much improved electrochemical performance including enhanced specific capacitance and charge-discharge cycles. The surface morphology, functionalities, crystallinity and electron microstructures were also investigated to fully understand the material and its synthesis mechanism.

2. Experimental section

2.1. Materials

Graphite was obtained from Jingchun Co., Ltd. (Shanghai, China). Aniline (99.5%) was purchased from Aladdin and distilled under reduced pressure prior to use. Gold chloride ($\text{HAuCl}_4 \cdot 4\text{H}_2\text{O}$), Chitosan (Cs) and ammonium peroxydisulfate (APS) were purchased from Sinopharm Chemical Reagent Co., Ltd (China).

Double distilled water was used throughout the experiments.

2.2. Synthesis of Binary GA

Graphene oxide (GO) was prepared using a modified Hummer's method.^[27,28,29] First, a mixture of graphite powders and KMnO_4 were added to a mixture of H_2SO_4 and H_3PO_4 (v/v=9:1), which caused the temperature slightly increased to 35–40 °C. Then the mixture was heated to 50 °C and stirred overnight. The mixture was cooled to RT and poured onto ice (400 mL) with 30% H_2O_2 (3 mL). After that, the mixture was centrifuged at 4000 rpm for 20 min and the supernatant was decanted away. The solid material was washed with HCl, ethanol, and ultrapure water until the pH of the washing solution was neutral. The achieved graphene oxide was dried overnight. Graphene oxide powder was dispersed in ultrapure water by ultrasonication for 1 h and subsequently centrifuged for 15 min at 3000 rpm and dried overnight. GO was synthesized successfully.

A typical experiment for the synthesis of binary graphene/Au (GA) nanocomposite is as follows: GO (50 mg) was dispersed in 100 mL ultrapure water by ultrasonication for 1 h, 10 mL HAuCl_4 (1 wt%) was added to the solution under vigorous stirring. Then, sodium citrate (1.0 g) was added to the mixture. The resulting mixture was heated to 95 °C and kept stirring at that temperature for overnight.

2.3. Synthesis of Ternary GAP Nanocomposites

Ternary graphene/Au/PANI (GAP) was synthesized via in situ polymerization of aniline monomers in the presence of binary GR-Au. The extracted binary GR-Au nanocomposite and ammonium peroxydisulfate (APS, 5 mmol) were dispersed in 50

mL of 2 M HCl aqueous solution with ultrasonic vibrations for 30 min to obtain a uniform suspension. Aniline (5 mmol, 0.1 M) was then added into this mixture dropwise under vigorous stirring in an ice-water bath, after which, the resulting mixture was allowed to polymerize under stirring for 10 h in the ice-water bath. Finally the ternary GAP_{0.1M} hybrid was filtered out and washed with a large amount of deionized water. The other ternary GAP hybrids (GAP_{2M}, GAP_{1M}, GAP_{0.5M}, GAP_{0.05M}) were also prepared with the same amount of GA.

2.4. Fabrication of Supercapacitor Electrodes

The supercapacitor electrode was prepared by casting a CS (Chitosan)-impregnated sample onto a glassy carbon electrode with a diameter of 5 mm. The bared glassy carbon working electrode (GCE) was polished with 0.3 and 0.05 μm alumina slurry, and then thoroughly washed in ethanol and ultrapure water, respectively. The electrode material (10 mg) was dispersed in 1 mL of 0.5 wt% CS under sonication to obtain a homogeneous suspension. This dispersion (30 μL) was then dropped onto the glassy carbon electrode and dried in air. Next, another 30- μL dispersion was dropped onto the dried electrode surface and dried in air before electrochemical testing.

2.5. Characterization

The morphology of the GR-Au and GAP nanocomposites was characterized by a QUANTA PEG 250 field emission scanning electron microscope (SEM) and a JEM-2100 high resolution transmission electron microscope (TEM). Powder X-ray diffraction (XRD) data were obtained on a Bruker D8 advanced X-ray diffractometer

using Cu K α radiation at a scan of 0.02 °/s and the diffraction data were recorded for 2 θ angles between 2° and 80°. The FTIR spectrum was measured on a Nicolet Avatar 370 DTGS (Nicolet, USA).

A three-electrode cell system was used to evaluate electrochemical performances. Cyclic voltammetry (CV) and galvanostatic charge/discharge measurements were carried out with a CHI 760E electrochemical workstation (Chenhua Instruments Co., Shanghai, China) while the electrochemical impedance spectroscopy (EIS) was performed with a Zennium electrochemical workstation (Zahner, Germany). Sulfuric acid solution (2 M) was used as the electrolyte. A platinum wire and a KCl saturated Ag/AgCl electrode were used as the counter and the reference electrode, respectively. CV curves were recorded between -0.2 and 0.6 V vs Ag/AgCl at different scan rates. Galvanostatic charge/discharge tests were performed at current densities of 0.1, 0.2, 0.5, 1, 2, 3 and 5 A/g. EIS measurement was carried out at open circuit potential with AC amplitude of 20 mV over the frequency range from 100 kHz to 0.1 Hz. The specific gravimetric capacitance was calculated from the discharge process according to the following equation^[21]:

$$C = \frac{I\Delta t}{m\Delta V} \quad (1)$$

Where C is the specific capacitance of the active material (F/g), I is the applied current (A), Δt is the total charge-discharge time (s), ΔV is the potential change (V), and m is the mass of active material (g) in the electrode.

3.RESULT AND DISCUSSION

3.1. Composition Analysis

The structures of GAP nanocomposite are characterized by the Fourier transformed infrared (FTIR) spectra, elemental analysis, and X-ray diffraction (XRD). FTIR spectra of pure PANI, GR-PANI, GR-Au and GAP are shown in Fig. 1a. The FTIR spectra of graphene (Fig.1b) and PANI are in good agreement with previous reports.^[30-33] The presence of different functionalities in graphene nanosheets is found at 1722 cm^{-1} (C=O), 1592 cm^{-1} (skeletal C=C), and 1194 cm^{-1} (C-OH). All of these observations are due to stretching vibrations. The intensity of all peaks of graphene corresponding to the oxygen containing groups is dramatically decreased when compared with those of GO.^[30,34] FTIR also confirms the success of the in situ polymerization process of PANI composites. The functional groups of PANI are found at around 3440 cm^{-1} (N-H stretching), 3000 cm^{-1} (C-H stretching), 1580 cm^{-1} (C=C stretching of the quinoid ring), 1483 cm^{-1} (C=C stretching of the benzenoid ring), 1303 cm^{-1} (C-H in-plane bending), 1109 cm^{-1} (C-C stretching), and 800 cm^{-1} (C-H out-of-plane bending peak).^[33,35,36] FTIR spectra of the GR-PANI and GAP composites contain the functional groups of both PANI and graphene with lower intensities. Some peaks of these two materials overlapping as they are somewhat broad.

As shown in Fig. 1c, there are two major weight losses in the TGA curve of the ternary $\text{GAP}_{0.1\text{M}}$ composites. The first weight loss below 200°C is due to the physically adsorbed water of the composites. The second weight loss in the range of $200\text{-}630^\circ\text{C}$ corresponds to the removal of doping anions from the polyaniline structure and degradation of the polyaniline chain and graphene.^[18] No noticeable change was

observed above 630 °C and the residue weight was about 10%, which can be ascribed to the remaining AuNPs. Thus the contents of graphene and PANI were estimated to be about 5.4% and 84.6%, respectively.

The specific surface area of composites was calculated on the basis of BET theory and is shown in Fig. 1d. It can be noticed that the BET specific surface area of the GAP_{0.1M} was determined to be as high as 532 m²/g, which is much higher than that of either the pure PANI (49 m²/g)^[21] or the pure graphene (268 m²/g)^[21].

The XRD diffraction patterns of pure PANI, binary graphene-PANI (GP), binary graphene-Au (GAu) and ternary GAP_(0.1M, 0.5M, 2M) nanocomposite are shown in Fig. 2a and b. The diffraction peaks at 38.1°, 64.5° and 77.5° correspond to (111), (220) and (311) planes of AuNPs, respectively. Moreover, an additional peak is observed around 43.9°, which is due to overlapping (200) reflection plane of Au, at 2θ=44.4°, with (100) plane of graphene. In addition, the broad diffraction peaks at about 15°, 21° and 25° are the features of doped PANI. As for binary GR-Au and GR-PANI nanocomposites, the diffraction peaks of AuNPs and PANI are observed without typical diffraction peaks of graphene, indicating that the stacks of graphene oxide were destroyed after the hydrothermal reaction^[37] and fully used as the substrate of AuNPs and PANI to produce hierarchical nanocomposites.^[38] In the XRD pattern of the ternary GAP_{0.1M} nanocomposite, the diffraction peaks of both AuNPs and PANI can be observed. This suggests that AuNPs and PANI coexist in the as-prepared ternary nanocomposite. The XRD diffraction patterns of ternary GAP nanocomposites with differing PANI content are shown in Fig. 2b. With increasing PANI content, the

diffraction peaks of AuNPs become weaker and broader.

3.2. Morphology of Composites

Fig. 3a shows the two-step synthesis process: (1) the exfoliation of GO in a diluted aqueous solution, followed by uniform mixing of GO and HAuCl_4 , and chemical reduction by sodium citrate; (2) GR-Au and aniline dispersed in water; the oxidation reaction by APS. The morphology of pure PANI and GAP were studied by SEM and TEM, as shown in Fig. 3b and Fig. 4. A layered structure has been observed in SEM image of GAP nanocomposites (Fig. 3b) and PANI nanorods (Fig. 3b (inset)) were anchored on the graphene sheets. It is speculated that, upon mixing GR-Au and PANI in the solution, the PANI nanowires tend to adsorb on the GR sheets due to the Coulombic interaction and van der Waals forces between PANI and GR-Au. Generally, when GO is reduced by the reductant, the hydrophilic functional groups on GO are removed, causing GR sheets to restack. In this work, most of absorbed PANI nanorods were sandwiched between layers of graphene. These PANI nanorods act as spacers to create gaps between neighboring graphene sheets. In addition, as shown in Fig. 3c-e, the energy dispersive X-ray spectrometry (EDS) mapping indicated that the Au, N, and C elements were distributed throughout the $\text{GAP}_{0.1\text{M}}$ samples.

Fig.4a-b display the TEM images of binary GR-Au with different magnifications, Au nanoparticles show an average size of about 20 nm and are distributed uniformly on graphene sheets. The TEM image of ternary $\text{GAP}_{0.1\text{M}}$ is shown in Fig.4d. Compared with the TEM image of pure PANI (Fig.4c), it can be seen that the aggregation of rods PANI almost disappeared in the ternary $\text{GAP}_{0.1\text{M}}$ composites,

indicating a high loading efficiency. Meanwhile, the graphene/Au nanocomposites can still be observed in the ternary nanocomposite, which reflects that Au nanocomposites supported by the graphene were stable during the in situ polymerization process. Overall, on the basis of SEM and TEM observations, it can be concluded that graphene/Au/PANI composites synthesized here exhibited a layered structure. Such a structure with both a high surface area and a uniform size distribution may lead to a faster diffusion rate in GAP composites, which can be utilized in supercapacitor applications.

3.3. Electrochemical Performance Measurement

To evaluate the electrochemical performance of the as-prepared composites in serving as active materials for supercapacitor electrodes, cyclic voltammetry (CV), galvanostatic charge/discharge and electrochemical impedance spectroscopy (EIS) measurements were performed in a three-electrode system. Fig. 5a presents the CV curves of pure PANI, binary GR-PANI, ternary GAP_{2M}, ternary GAP_{1M}, ternary GAP_{0.5M}, ternary GAP_{0.1M} and ternary GAP_{0.05M} nanocomposites. It is obvious that the ternary GAP nanocomposite shows the highest current density among all the electrode materials, implying its best capacitive performance. The high electrochemical performance of ternary GAP may result from the well-designed nanostructure and the synergistic effects among the three components. First, the addition of graphene can greatly improve the electrical conductivity and control the morphology and nanostructure of Au nanoparticles, which can further lead to high electrode/electrolyte contact areas and high rates of electrode reaction, resulting in

enhanced electrochemical performance. Second, PANI nanowires can remarkably increase the pseudo-capacitance contribution to the overall capacitance.^[39] Last, Au nanoparticles and PANI nanowires may prevent the restacking of the carbon sheets and provide Faradaic processes to increase the total capacitance. Besides, the π - π stacking, electrostatic interactions and hydrogen-bonding interactions between the PANI molecular chains and the graphene nanosheets are also beneficial for enhancing the electrochemical performance.^[40,41] Moreover, the content of graphene in the ternary composites plays an important role in the electrochemical performance. The electrochemical performance of ternary GAP composites with different mass of PANI was conducted under the same condition and the ternary GAP_{0.1M} shows the highest specific capacitance of 572 F·g⁻¹. Fig. 5b shows the CV curves of ternary GAP_{0.1M} at different scan rates. It is noted that the total peak current density of ternary GAP_{0.1M} increases obviously with increasing potential scan rate, demonstrating the good rate property and excellent capacitance behavior.

As can be seen in Fig. 6a, the long discharge time of ternary GAP nanocomposite indicates that it has the highest electrochemical performance. The galvanostatic charge/discharge curves of ternary GAP nanocomposites with differing graphene content are also shown in Fig. 6A and among them GAP_{0.1M} shows the highest capacity, which is in coincidence with the CV results. The electrochemical performance of ternary GAP composites with different mass of graphene was conducted under the same condition (Fig. 6B) and the ternary GAP_{0.1M} shows the highest specific capacitance of 482.5 F·g⁻¹.

Fig. 7A shows the galvanostatic charge/discharge curves of GAP_{0.1M} at different current densities. The time duration increases with the decrease in the current densities, while the charge/discharge curves keep a similar shape, revealing the sustainable behavior of the nanocomposite. According to the charge/discharge curves of different nanocomposites in the same current density range, the variations of the specific capacitance with the current density of these electrode materials are plotted together in Fig. 7B. The specific capacitance values of pure PANI and binary GR-PANI are much lower than the ternary composite. The binary GR-PANI possess high specific capacitance at low current density, while the specific capacitance is dramatically decreased from 437 to 198.97 F·g⁻¹ at current density of 0.1 - 5.0 A·g⁻¹. For GAP_{0.1M}, about 74.3 % of the specific capacitance was retained (from 572 to 425 F·g⁻¹) when the current density increased from 0.1 to 5.0 A·g⁻¹, which is more competitive than those of reference samples. These conclusions are further supported by the results from the EIS measurements, as shown in Fig. 7D. It can be seen that the charge transfer resistance in ternary GAP is lower than binary GR-PANI and pure PANI, proving again the faster rate of charge transfer on the GAP hybrid.

Cycling performance is another important factor in evaluating supercapacitor electrodes for practical applications. The electrochemical stability of the ternary GAP_{0.1M} nanocomposite was investigated at a current density of 1 A·g⁻¹ (Fig. 7C). After 10000 cycles, the GAP_{0.1M} electrode retained about 88.54% of initial capacitance, indicating superior capacity reversibility in consecutive charge/discharge cycles. The excellent stability of ternary GAP may be attributed to the well-designed

nanostructure and the synergistic effects among the three components of the ternary composite. Although PANI itself as a supercapacitor electrode shows poor cycling stability, the presence of graphene sheets can efficiently restrain the swelling and shrinkage of PANI during doping/dedoping processes, thus the hybrid material becomes more adaptable to volumetric changes during redox reaction. Besides, graphene undertakes some mechanical deformation in the redox process of PANI, and simultaneously PANI acts as a protective layer to stabilize the Au particles, both of which also help in improving the electrochemical stability.

4. Conclusion

In summary, a ternary graphene/Au/PANI (GAP) nanocomposite has been fabricated via a two-step approach. The as-synthesized ternary composites are characterized by XRD, morphology analyses and electrochemical measurements. It is found that the well-designed hierarchical nanostructure and the synergistic effects among the three components are conducive to the high electrochemical performance. The as-obtained ternary GAP composites exhibited a specific capacitance of $572 \text{ F}\cdot\text{g}^{-1}$ at a current density of $0.1 \text{ A}\cdot\text{g}^{-1}$, much higher than that of pure PANI. Even at $5 \text{ A}\cdot\text{g}^{-1}$, the capacitance of the composites was still $425 \text{ F}\cdot\text{g}^{-1}$. Our results have shown that ternary $\text{GAP}_{0.1\text{M}}$ nanocomposites possess superior electrochemical performance as supercapacitors.

Acknowledgments

This work is supported by the National Natural Science Foundation of China

(51003040), Shandong Provincial Natural Science Foundation, China (ZR2012BL11), and Shandong Provincial Science and Technology Development Plan Project, China (2013GGX10705).

Author Information

Corresponding Author

E-mail: chm_wangly@ujn.edu.cn; suying.wei@lamar.edu

Phone: Tel: +86-531-89736800 (L. W.); 409-880-7976 (S. W.)

Fax: +86-531-87161600 (L. W.); 409-880-8267 (S. W.)

References

- [1] Simon, P.; Gogotsi, Y. *Nat. Mater.* **2008**, 7, 845-854.
- [2] Zhang, L. L.; Zhao, X. S. *Chem. Soc. Rev.* **2009**, 38, 2520-2531.
- [3] Liu, C.; Li, F.; Ma, L.P.; Cheng, H.M. *Adv. Mater.* **2010**, 22, E28-E62.
- [4] Nyholm, L.; Nystrom, G.; Mihranyan, A.; Stromme, M. *Adv. Mater.* **2011**, 23, 3751-3769.
- [5] Meng, C.; Liu, C.; Chen, L.; Hu, C.; Fan, S. *Nano Lett.* **2010**, 10, 4025-4031.
- [6] Wu, Q.; Xu, Y.; Yao, Z.; Liu, A.; Shi, G. Q. *ACS Nano* **2010**, 4, 1963-1970.
- [7] Huang, J.; Wang, K.; Wei, Z. *J. Mater. Chem.* **2010**, 20, 1117-1121.
- [8] Li, C.; Bai, H.; Shi, G.Q. *Chem. Soc. Rev.* **2009**, 38, 2397-2409.
- [9] Ryu, K. S.; Kim, K. M.; Park, N. G.; Park Y. J.; Chang, S. H. *J. Power Sources*

2002, 103, 305–309.

[10] Zhou, S.; Zhang, H.; Zhao, Q.; Wang, X.; Li, J.; Wang, F. *Carbon*, **2013**, 52, 440–450.

[11] Sawangphruk, M.; Kaewsongpol, T. *Mater. Lett.* **2012**, 87, 142–145.

[12] Wang, H. L.; Hao, Q. L.; Yang, X. J.; Lu, L. D.; Wang, X. *Nanoscale*. **2010**, 2, 2164-2170.

[13] Fan, H. S.; Wang, H.; Zhao, N.; Zhang, X. L.; Xu, J. *J. Mater. Chem.* **2012**, 22, 2774-2780.

[14] Jiang, H.; Lee, P.S.; Li, C. *Energy Environ. Sci.* **2013**, 6, 41-53.

[15] Kovalenko, I.; Bucknall, D.G.; Yushin, G. *Adv. Funct. Mater.* **2010**, 20, 3979-3986.

[16] Sun, M.; Wang, G.; Li, X.; Cheng, Q.; Li, C. *Ind. Eng. Chem. Res.* **2012**, 51, 3981-3987.

[17] Sumboja, A.; Wang, X.; Yan, J.; Lee, P. S. *Electrochim. Acta* **2012**, 65, 190-195.

[18] Xiong, P.; Huang, H. J.; Wang, X. *Journal of Power Sources*. **2014**, 245, 937-946.

[19] Allen, M. J.; Tung, V. C.; Kaner, R. B. *Chem. Rev.* **2010**, 110, 132-145.

[20] Huang, X.; Qi, X.; Boey, F.; Zhang, H. *Chem. Soc. Rev.* **2012**, 41, 666-686.

[21] Li, Z. F.; Zhang, H. Y.; Liu, Q.; Sun, L. L.; Stanciu, L.; Xie, J. *ACS Appl. Mater. Interfaces* **2013**, 5, 2685–2691.

[22] Kumar, N. A.; Baek, J. B. *Chem. Commun.* **2014**, 50, 6298--6308.

[23] Nam, S. H.; Shim, H. S.; Kim, Y. S.; Dar, M. A.; Kim, J. G.; Kim, W. B. *ACS*

Appl. Mater. Interfaces **2010**, 2, 2046-2052.

[24] Zhu, J.; Xu, Z.; Lu, B. G. *Nano Energy* **2014**, 7, 114-123.

[25] Buffat, Ph.; Borel, J.-P. *Phys. Rev. A* **1976**, 13, 2287.

[26] Koga, K. J.; Ikeshoji, T.; Sugawara, K. I. *Phys. Rev. Lett.* 2004, 92, 115507.

[27] Hummers, W. S.; Offeman, R. E. *J. Am. Chem. Soc.* **1958**, 80, 1339-1339.

[28] Kovtyukhova, N. I.; Olivier, P. J.; Martin, B. R.; Mallouk, T. E.; Chizhik, S. A.; Buzaneva, E. V.; Gorchinskiy, A. D. *Chem. Mater.* **1999**, 11, 771-778.

[29] Pan, N.; Guan, D.; Yang, Y.; Huang, Z.; Wang, R.; Jin, Y.; Xia, C. *Chem. Eng. J.* **2014**, 236, 471-479.

[30] Sawangphruk, M.; Srimuk, P.; Chiochan, P.; Krittayavathananon, A.; Luanwuthi, S. *Carbon* **2013**, 60, 109-116.

[31] Jiang, Y.; Zhang, Q.; Li F.; Niu, L. *Sens. Actuators, B* **2012**, 161, 728-733.

[32] Bal Sydulu, S.; Palaniappan, S.; Srinivas, P. *Electrochim. Acta* **2013**, 95, 251-259.

[33] Patil, D. S.; Shaikh, J. S.; Dalavi, D. S.; Kalagi S. S.; Patil, P. S. *Mater. Chem. Phys.* **2011**, 128, 449-455.

[34] Zhou, X.; Zhang, J.; Wu, H.; Yang, H.; Zhang, J.; Guo, S. *J. Phys. Chem. C* **2011**, 115, 11957-11961.

[35] Liu, H.; Wang, Y.; Gou, X.; Qi, T.; Yang, J.; Ding, Y. *Mater. Sci. Eng. B* **2013**, 178, 293-298.

[36] Sawangphruk, M.; Suksomboon, M.; Kongsupornsak, K.; Khuntilo, J. *J. Mater. Chem. A* **2013**, 1, 9630-9636.

[37] Fu, Y.; Chen, H.; Wang, X. *Appl. Catal. B* **2012**, 111-112, 280-187.

- [38] Xu, J. J.; Wang, K.; Zu, S. Z.; Han, B. H.; Wei, Z. X. *ACS NANO* **2010**, 4, 5019-5026.
- [39] Lu, X.; Dou, H.; Yuan, C.; Yang, S.; Hao, L.; Zhang, F.; Shen, L.; Zhang, L.; Zhang, X. *J. Power Sources* 197 (2012) 319-324.
- [40] Wang, H.; Hao, Q.; Yang, X.; Lu, L.; Wang, X. *ACS Appl. Mater. Interfaces* 2010, 2, 821-828.
- [41] Zhong, M.; Song, Y.; Li, Y.; Ma, C.; Zhai, X.; Shi, J.; Guo, Q.; Liu, L. *J. Power Sources* **2012**, 217, 6-12.

Figures

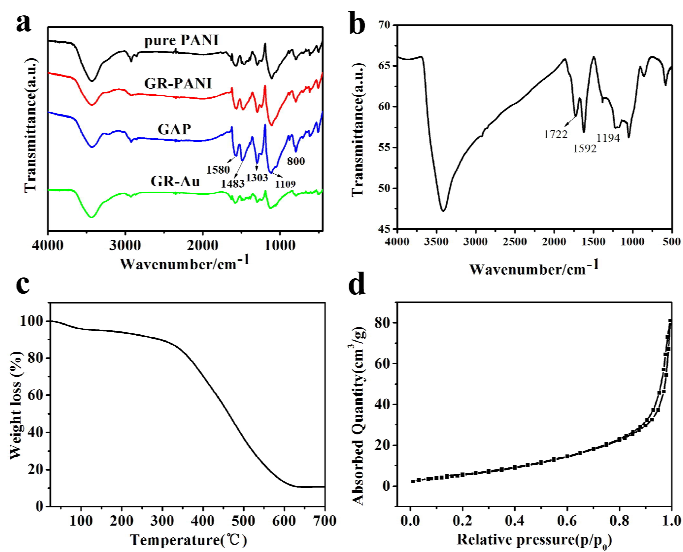


Fig.1

Figure 1. FTIR spectra of (a) pure PANI, GR-PANI, GAP_{0.1M} and GR-Au; (b) graphene. (c) TGA analysis of the ternary GAP_{0.1M} composites. (d) N₂ adsorption/desorption isotherms.

Fig.2

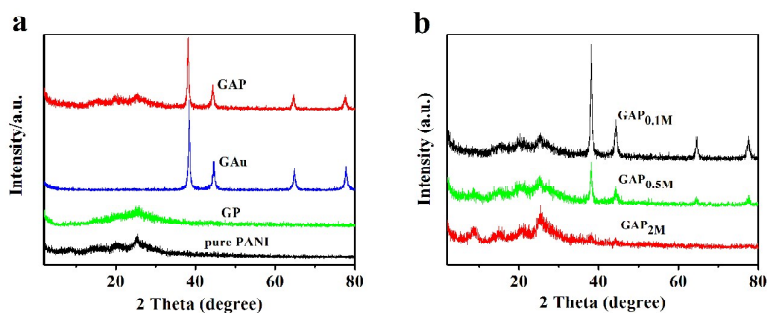


Figure 2. XRD patterns of (a) pure PANI, binary GP, binary GAu and ternary GAP_{0.1M} nanocomposites; (b) XRD patterns of different ternary GAP nanocomposites

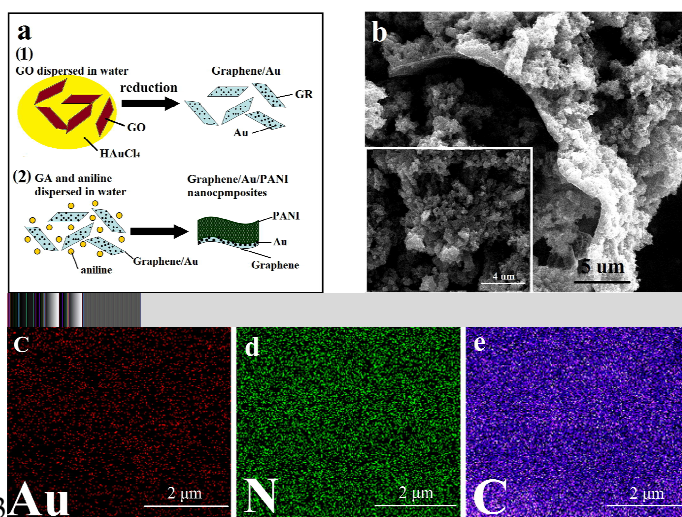


Fig.3

Figure 3. (a) Schematic illustration of the preparation of Graphene/Au and Graphene/Au/PANI, (b) SEM image of ternary GAP nanocomposite and pure PANI (inset of b), and the element mapping of Au, N, C acquired from (c-e).

Fig.4

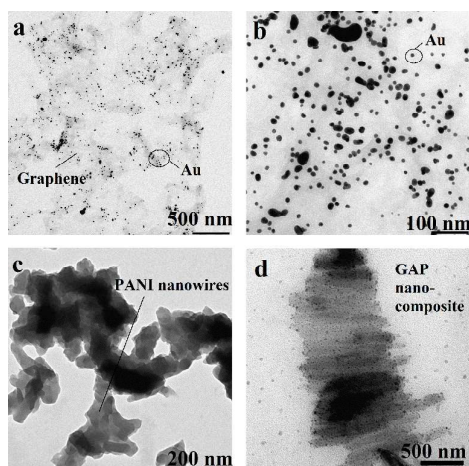


Figure 4. TEM images of binary GR/Au (a, b is a enlarged image of part of a), pure PANI (c) and ternary GAP_{0.1M} (d).

Fig.5

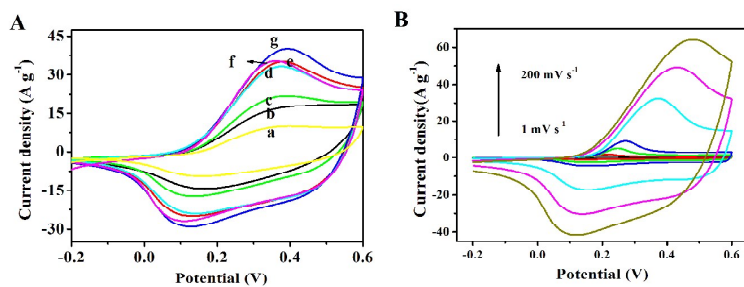


Figure 5. (A) CV curves of pure PANI (a), binary GR-PANI (b), ternary GAP_{2M} (c), ternary GAP_{1M} (d), ternary GAP_{0.5M} (f), ternary GAP_{0.1M} (g) and ternary GAP_{0.05M} (e) in 1 M H₂SO₄ at 100 mV·s⁻¹. (B) CV curves of ternary GAP_{0.1M} nanocomposites at different scan rates in 1 M H₂SO₄.

Fig.6

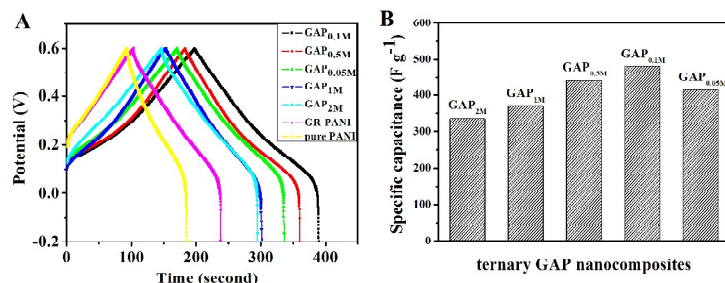


Figure 6. (A) Galvanostatic charge/discharge curves of pure PANI, binary GR-PANI, and different ternary GAP at $1 \text{ A}\cdot\text{g}^{-1}$, (B) Specific capacitances of different ternary GAP at $1 \text{ A}\cdot\text{g}^{-1}$.

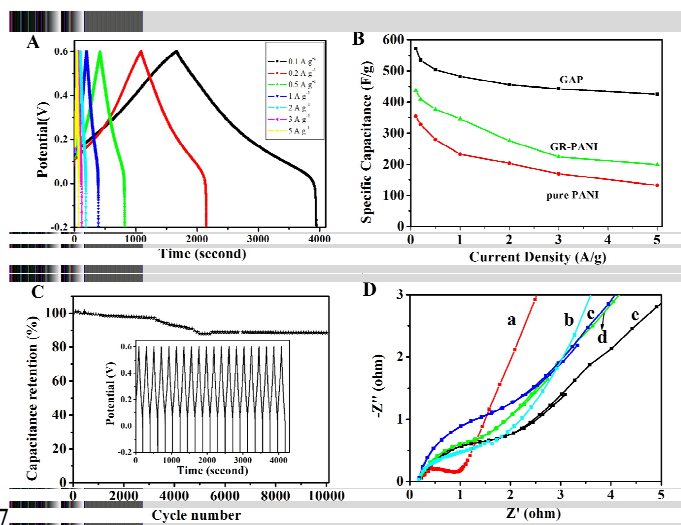
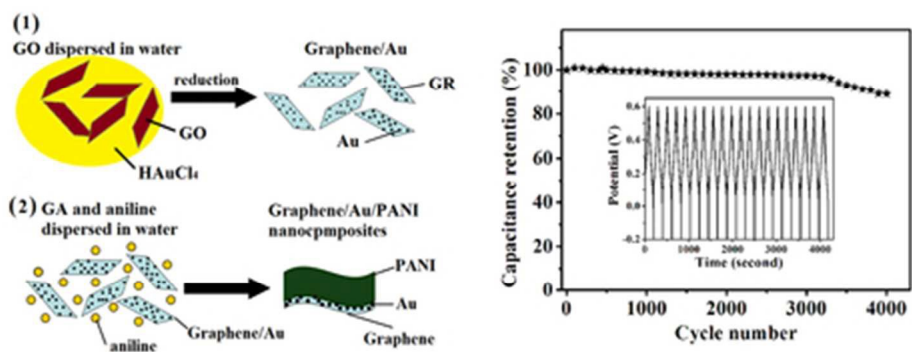


Fig. 7 (A) Galvanostatic charge/discharge curves of ternary $\text{GAP}_{0.1\text{M}}$ nanocomposites at different current densities. (B) Variation of the specific capacitance with current density for pure PANI, binary GR-PANI and ternary $\text{GAP}_{0.1\text{M}}$ nanocomposites. (C) Cycle stability of ternary $\text{GAP}_{0.1\text{M}}$ nanocomposites during the long-term charge/discharge process at a current density of $1 \text{ A}\cdot\text{g}^{-1}$, the inset showing the typical charge/discharge curves. (D) EIS measurement of ternary $\text{GAP}_{0.1\text{M}}$ (a), ternary $\text{GAP}_{0.5\text{M}}$ (b), pure PANI (c), binary GR-PANI (d) and ternary $\text{GAP}_{0.05\text{M}}$ (e).



40x16mm (300 x 300 DPI)